



CHORUS

This is the accepted manuscript made available via CHORUS. The article has been published as:

Manipulating Abrikosov vortices with soft magnetic stripes

V. K. Vlasko-Vlasov, F. Colauto, A. I. Buzdin, D. Rosenmann, T. Benseman, and W.-K. Kwok

Phys. Rev. B **95**, 174514 — Published 22 May 2017

DOI: [10.1103/PhysRevB.95.174514](https://doi.org/10.1103/PhysRevB.95.174514)

Manipulating Abrikosov vortices with soft magnetic stripes

V. Vlasko-Vlasov, F. Colauto, A. I. Buzdin, D. Rosenmann, T. Benseman, W.-K. Kwok

Tuning the polarization of a periodic array of magnetic stripes on top of a superconducting film allows control of Abrikosov vortex motion. Using direct magneto-optical imaging of the vortex patterns, we demonstrate that the proximity of the magnetic stripe ends to the edges of the superconducting film can strongly alter the vortex dynamics. We observe qualitatively different vortex behavior when the stripes overlap with the film edges. From the resulting unique magnetic flux patterns, we calculate the magnetic pinning strength of our stripe array and study effects of the modified edge barrier on vortex guidance and gating that result from different polarizations of the stripes .

1. Introduction

Development of new low power micro-circuitry is a crucial requirement for future digital information technologies [1-6]. Superconducting materials capable of transferring electric signals without dissipation provide a potential solution towards this goal. Furthermore, Abrikosov vortices, representing spatially isolated single magnetic flux quanta in superconductors (SC), can be inherent carriers of digital information in advanced microprocessors and memories. Although numerous projects involving vortices for computation have been discussed for some time, and original vortex storage devices have been demonstrated (see [7] and refs there), there are no established protocols for the reliable control of individual Abrikosov vortices. In our recent works [8-9] we demonstrated that arrays of thin soft ferromagnetic (FM) stripes, where the in-plane magnetization easily turns with a small applied in-plane field, can be used to manipulate vortices at small length-scales. By rotating the magnetic polarization of permalloy stripes placed on top of a niobium superconducting film, the magnetic charges at the edges of the stripes can be adjusted to act as guides or strong barriers for vortex motion in the underlying superconducting film. The variable magnetic potential at the stripe edges introduces a tunable anisotropy to the vortex motion in a way similar to the gate electrode in an electronic triode. As a follow-on to these previous studies, in our new work we show that the proximity of the ends of the magnetic strips to the edge of the underlying SC film has a profound effect on vortex motion. We find that the flux behavior changes qualitatively when the ends of the FM stripes overlap with the edges of the superconductor. The ubiquitous edge barrier for vortex entry is modified in this case and facilitates unrestricted flux penetration. From magneto-optical experiments, we obtain the ratio of the supercurrents in the areas with and without the magnetic strips and estimate the magnetic pinning at the stripe edges. Below, we present the vortex patterns from various in-plane stripe polarization and discuss the dominant physical forces responsible for the vortex dynamics in our hybrid FM/SC structure.

There is a vast literature on different SC/FM designs and they are thoroughly discussed in widely cited review articles [10-12] and books [13]. References on recent studies of FM/SC hybrids can be found in [14-18]. In this work, we focus on the effects of soft magnetic stripes on vortex dynamics, which we posit can lead to the manipulation of single Abrikosov vortices.

2. Sample and experiment

Similar to our previous FM/SC hybrid samples with stripe arrays [8- 9], we deposited 40 nm thick ferromagnetic permalloy (Py) stripes onto a 100 nm thick niobium (Nb) film. The Nb ($T_c=8.7\text{K}$) was sputtered onto laser lithography defined 2×2 mm square on silicon substrate using a high-vacuum magnetron system. To avoid SC/FM proximity effects, the Nb film was covered with a 15nm thick SiO_2 layer using a plasma enhanced chemical vapor deposition setup. Subsequently, e-beam lithography was used to pattern arrays of $30 \mu\text{m}$ wide parallel stripes with $2 \mu\text{m}$ gaps, followed by magnetron sputtering deposition of Py and lift-off. The stripes possess in-plane magnetization with practically no in-plane anisotropy. Here, unlike in our previous studies, the Py stripes were placed $200 \mu\text{m}$ away from three sides of the Nb square film and overlapped with the fourth side of the Nb square film (see Fig.1). This arrangement allowed us to simultaneously study the effect of overlapping and non-overlapping magnetic stripe edges on flux dynamics.

We used our Magneto-optic (MO) indicator technique [19] to directly image the normal-flux dynamics in the sample at $T < T_c$ while cycling the magnitude of the perpendicular magnetic field, H_z . The Py stripes were polarized along different directions within the film plane by applying an in-plane magnetic field $H_{||}$ (20 to 150 Oe) at $T > T_c$. The sample was field cooled in a constant $H_{||}$ to a selected temperature below T_c , and images of the normal flux distribution, $B_z(x,y)$, were taken at different values of applied H_z while $H_{||}$ was kept unchanged. The MO images of the stray fields emanating from the in-plane magnetized Py stripe edges were subtracted from the images obtained with H_z to reveal only the entering vortices generated by the normal field.

2. Results and discussion

2a. Transverse polarization of Py stripes

When the applied in-plane field, $H_{||}$, magnetizes the Py stripes *transverse* to their length, the resulting stray fields emanating from their long edges form a periodic pattern with up and down components as shown in Fig.2. Since the thickness, d_f , of the stripes is much smaller than their width W and the gap D , the stray fields can be described as those diverging radially from a set of linear magnetic monopoles with alternating magnetic charge signs placed at neighboring stripe edges. The magnetic charge is provided by a jump in the normal component of the magnetization \vec{M} at the stripe edge, which yields a magnetic charge density $\rho_m = -\text{div}\vec{M}$. The charge per unit length at the edge is $\sigma_m = \pm M d_f$, and the strength of the radial stray field at a distance R from the edge is $H_s = \sigma_m / 2\pi R$. In the gap region, the total \vec{H}_s will be comprised of a combination of fields due to the oppositely charged neighboring edges (for $W \gg D$ the contribution from distant gaps is negligible). Treating the Abrikosov vortex as a point magnetic charge $m = 2\Phi_0$ [20], the force on the vortex crossing the gap due to two oppositely charged magnetic lines will be (see Fig.3a):

$$F_{mv} = \frac{m\sigma_m}{2\pi} \left[\frac{R}{R^2+h^2} + \frac{D-R}{(D-R)^2+h^2} \right] \quad (1)$$

Here h is the height of both lines above the SC film, R is the distance of the vortex from the projection of left (positive) charged line on the SC film, and $D-R$ –distance from the right (negative) charged line projection. Thus positive vortices will be repelled with a force $\sim 1/R$ from the positively charged stripe edge and attracted towards the negatively charged edge. The $1/R$ dependence of F_{mv} will be modified if we account for the Meissner currents induced in the SC thin film by the stray fields, H_s . Within the London approximation, the analytical formula for the force on the vortex in the gap region is [9]:

$$F(R) = \frac{c\Phi_0 M d_f}{2\pi\lambda_{eff}} \left[f\left(\frac{R+D}{2\lambda_{eff}}\right) - f\left(\frac{R}{2\lambda_{eff}}\right) \right] \quad (2)$$

where $f(x) = \int_0^\infty \frac{\sin qx}{1+q} dq = Ci(x)\sin x - Si(x)\cos x + \frac{\pi}{2}\cos x$, $\lambda_{eff}=\lambda^2/d$

and $Ci(x) = -\int_x^\infty \frac{\cos t}{t} dt$, and $Si(x) = \int_0^x \frac{\sin t}{t} dt$ are cosine and sine integrals.

This more accurate solution reduces the force on the vortex at short distances from the stripe edges (see Fig.3b) compared to eq.1, although the qualitative picture remains the same. Appropriate potentials for the vortex/edge interactions, $U(R)=-\int FdR$, show the same tendency (see Fig.3c). Similar approach was used in [Vestgargen et al. 21] for analysis of the vortex interactions with charged domain walls in the magnetic garnet film placed on top of the superconducting layer.

Another factor that should be considered in the description of the vortex/magnetic stripe interaction is the presence of field-cooled vortices generated by the Py edge stray fields (H_s) upon cooling the sample below T_c . In the vicinity of the positively charged edge, these H_s induced vortices have negative polarity and at the negatively charged edge they have positive polarity as shown in Fig.2. Therefore, the force from these H_s induced vortices on the H_z created vortices should be opposite to that of the magnetically charged edges. Namely, near the positive edge, the H_s -vortices will attract H_z -vortices, and near the negative edge they will repel the H_z -vortices. The resulting motion of the H_z -vortices at the initial stage of magnetization will be defined by their interactions with the magnetically charged stripe edges, with the H_s -vortices residing close to these edges, and with the intrinsic pinning centers in the superconducting film. Note that forces between point charges of H_s - and H_z -vortices ($\sim 1/R^2$) decay faster than forces between H_z -vortices and filaments of edge charges F_{mv} ($\sim 1/R$), and should be important only for H_z -vortices in close proximity to the stripe edges. Moreover, the H_s -vortices can be important only at very small H_z . At later stages of the magnetization, the negative H_s -vortices will be annihilated by the incoming H_z -vortices, while positive H_s -vortices will be only a small part of the total B_z , and the effect of the charged stripe edges will be the dominant factor. Below, we show how the above scenario unfolds in the experiment.

Fig.4 presents successive images of the normal flux entry with increasing H_z at $T=5K$. At small fields, the screening currents in the bare Nb film regions along the top, left and right sides of the sample prevent flux from entering the film, whereas there is pronounced vortex entry from the bottom side, where the Py stripes reach the edge of the Nb square. Here, bright streaks appear, associated with the H_z -vortices entering along the inter-stripe gaps (Fig.4a). With increasing H_z , the normal vortices propagate deeper into the sample along the gaps. Simultaneously, small irregular shaped flux lobes of H_z -vortices begin to appear at the other edges of the Nb square (Fig.4b). When these lobes that extend from the top sample edge approach the ends of the Py stripes, they form a sharp front modulated by

the Py stripe pattern periodicity and narrow streaks of vortices stretch along the inter-stripe gaps ahead of this front (Fig.4c). The fine features of the vortex distribution near the top stripe ends are very similar to those observed and discussed in detail in [9]. In fact, before the sharp front reaches the top edge of the Py pattern, we observe accumulation of negative H_s -vortices at the short stripe ends, which are pushed towards the advancing front of positive H_z -vortices with increasing Meissner currents (see [9]). With further increase of H_z , the negative H_s -vortices are annihilated by the entering H_z -vortices and new positive vortices propagate inside the stripe gaps. At even higher fields, the vortex streaks spreading from the top and bottom sides meet at a horizontal line (dark line in Fig.4d) located above the center of the sample. The position of this line reflects the earlier penetration of the normal flux from the bottom side of the sample where Py stripes overlap with the Nb film edge. On the left and right sides of the sample, vortices accumulate at the long stripe edges (brighter lines) forming a terraced structure (Fig.4d). The first accumulation on the left side starts at the left-most positively charged Py stripe edge. However, on the right, the accumulation occurs not at the right-most (negatively charged) stripe edge, but at the next inter-stripe gap. We observed similar asymmetry in [9] and explained it by different action of the potential barrier formed at the positively charged Py stripe edge and potential valley at the negatively charged edge on the vortex dynamics. In the Appendix, we model the overdamped vortex motion across the sharp 1D repulsive and attractive potentials of identical strength. The resulting vortex trajectories $X(t)$ show that in spite of the same value of the static pinning forces produced by both potentials, moving vortices can more easily cross the edges with the attractive potential. This confirms the dynamic nature of the asymmetry.

Another possible explanation of the asymmetry could be partial compensation of the negative effective charge σ_m^- at the attractive magnetic stripe edge from the entering positive vortices and appropriate enhancement of σ_m^+ at the repulsive edge. However, since the saturation magnetization of Py ($M_s \sim 800$ G) is much larger than the normal fields in Fig.4, this effect seems to be secondary.

With further increasing H_z , the normal flux occupies the entire sample, forming an off-centered envelope pattern of the critical state (Fig.4e). Here, the minimum B_z occurs along the lines of sharp current turns (SCT) where the average critical currents J_c abruptly change direction (dark lines in Fig.4e). Such SCT-lines are typical for thin SC plates and films of regular shapes and allow estimates of the current anisotropy in the sample. In the bare Nb film corners (top left and right), the SCT-lines follow the bisectors of the square indicating *isotropic* J_c at these corners. However, in regions of Nb film under the Py magnetic pattern the currents are anisotropic and the SCT-lines tilt. From the SCT-line angles (as shown in Fig.4e), we can extract the ratio of the average currents along and across the stripes, $k = J_c^{\parallel} / J_c^{\perp} \sim 2.6$ at $T=5$ K. This *anisotropy* decreases slightly with field and substantially increases with temperature, as we also observed for samples with larger inter-stripe gaps [9].

A new tilt in the SCT lines appears at the corners of the sample on the side where the Py stripes overlap the Nb film edge (bottom left and right corners). From the geometry of the SCT-lines formed in these corners, it is possible to extract the ratio of the current flowing across the Py stripes in the patterned area ($J_{c2} = J_c^{\perp}$) and the current in the bare Nb film ($J_{c1} = J_c^{\text{Nb}}$) as schematically shown in Fig.5. Using the ratio of $J_c^{\parallel} / J_c^{\perp}$ obtained from the

angles of the SCT lines in the patterned area, we can obtain the relationship between all three current densities $J_{c\parallel}$, $J_{c\perp}$, and $J_{c^{Nb}}$. In Fig.6 we present snapshots of the SCT line positions at the right edge of the sample at several temperatures with increasing (top row) and decreasing (bottom row) normal fields, H_z . Locations of the horizontal SCT lines and points of their crossing with tilted SCT lines in the patterned area are indicated by small green and red circles, respectively. Crossings of the tilted SCT line in the bare Nb region with the edge of the pattern is indicated with a short yellow arrow. One can see that the horizontal SCT line moves up and expands to the right with increasing temperature. Also, the tilted SCT line in the bare Nb region (yellow arrow) extends up with temperature. Such a behavior is a consequence of the temperature variation of the critical current anisotropy. The ratios of the critical currents extracted from the MO pictures are shown in Fig.7, where we present all three ratios between different J_{ci} . At $T > 7K$ the SCT lines in the MO images are poorly defined but the enhancement of the critical current anisotropy under the Py stripes is certain, and underlines the increased role of magnetic pinning at higher temperatures. Interestingly, $J_{c\parallel} / J_{c\perp}$ increases strongly with T , while $J_{c^{Nb}} / J_{c\perp}$ changes more gradually and the ratio of $J_{c\parallel} / J_{c^{Nb}}$ varies even slower. This could be explained by the relatively small total number of Py stripe edges in the patterned area, which act as the main channels for vortex guiding or as pinning barriers responsible for the anisotropy. The values of all the above J_c ratios are >1 indicating that the average current across the stripes is always smaller than in the pure Nb film, and currents along the stripes are always larger than $J_{c^{Nb}}$. We associate the relative reduction of $J_{c\perp}$ with the meandering current trajectories due to their bending near the Py stripe edges, which promotes vortex motion along these edges (see Fig.3 in [9]). In turn, the magnetic pinning by the edges preventing the vortex motion across them is responsible for the enhanced $J_{c\parallel}$.

Another effect associated with the Py stripes is the zigzag deformation of the tilted SCT lines when segments of the SCT lines are confined along the stripes. It is defined by inhomogeneity of the current density flowing along the stripes, $J_{c\parallel}(x)$, which is maximum at the stripe edges and decreases away from the edges. With increasing temperature, the length of the SCT line segments aligned with the stripe edges increases (see e.g. top row of pictures in Fig.6) confirming the enhanced role of magnetic pinning at larger T . At $T \sim 8K$ it is nearly impossible to identify distinct SCT-lines.

2b. Longitudinally polarized Py stripes

When the Py stripes are magnetized along their length, magnetic charges form at their short ends. This yields a dashed line of positive (or negative, depending on direction of H_{\parallel}) charges residing directly at the bottom edge of the Nb square. A similar line of opposite charges forms at the opposite ends of the Py stripes, at a distance of 200 μm from the top Nb film edge. Consequently, the short ends of the stripes should act as a potential barrier or valley for vortices generated by the applied normal field, H_z , depending on the sign of the magnetic charges and polarity of H_z . Concurrently, the gaps between the Py stripes should only moderately interfere with the normal flux entry, facilitating a gate-like action [8-9]. Our sample design allows simultaneous comparison of the gate-like behavior of the periodic stripe ends that are located at a distance from the Nb edge (top side of sample) and those placed directly at the edge (bottom side of the sample).

Fig. 8 shows the entry of H_z -induced flux at 5K for the sample with longitudinally magnetized stripes. For the chosen polarity of $H_{||}$, the negatively charged stripe ends at the bottom side of the sample do not show any noticeable effect on vortices. Namely, the flux penetration here is the same as that in the bare Nb film region at the top side of the sample (Fig.8a). However, we observe a pronounced effect of the Py stripes at the top side when the vortex front advancing from the top sample edge approaches the positively charged stripes ends. Here the MO images show a strong delay and accumulation of H_z - vortices at the stripe ends as evinced by the high contrast horizontal line in the MO image of Fig. 8b. Dark triangles on the other side of this line reveal regions with reduced vortex density behind the Py stripe ends. At the same time, vortices enter into the gaps between the stripes and form flux-lobes that extend along the gaps and expand laterally under the Py stripes. In fact, the gaps act as gates for vortices allowing only reduced flux entry *across* the line of positively charged stripe ends. For more details of normal flux penetration across the positively charged Py stripe ends, see [8-9]. At larger fields, the flux lobes spread deeper and form a smooth B_z front, leaving a “diamond-like” pattern of bright/dark contrast at the stripe ends (Fig.8c). These diamond-like patterns corresponding to increased supercurrents along the stripe ends indicate that strong magnetic pinning at the positively charged ends remains up-to high magnetic fields. As we have already observed in [8-9], if the longitudinal stripe polarization is inverted, the negatively charged stripe ends away from the Nb film edges do not affect positive vortex entry. This is similar to the asymmetry observed for vortex entry across the long edges of the transversely polarized stripes. As discussed above, the strong vortex delay at the positively charged Py stripe edges and negligible effect of the negatively charged stripe edges result in a peculiar vortex dynamics. The positive vortices are slowed down by the positively charged magnetic edges and stop in front of the potential barrier. However these vortices accelerate towards the negative edge and easily cross it. Actually, vortices are delayed in both cases (see Appendix), but the delay by the attractive barrier is less pronounced and the probability of the vortex transit across it is considerably higher. In addition, the heat released due to vortex acceleration towards the negatively charged Py stripe edge could be another factor assisting the barrier crossing.

On the left and right sides of the sample, longitudinally polarized stripes do not show any effect on vortex entry. This is expected, since here the long stripe edges are “neutral” (uncharged) and hence the vortex-stripe interactions are very weak, so that the motion of H_z -vortices is defined only by pinning from inherent defects in the Nb film.

In the total critical state formed at larger H_z , when vortices occupy the entire sample (Fig.8d), the SCT lines follow diagonals of the Nb square, demonstrating that the average critical currents along and across the magnetically neutral long stripe edges are practically the same and currents under the Py pattern are the same as in the bare Nb film. A small anisotropy with preferential vortex motion across the stripes, probably due to modulations of the stripe magnetization by the vortex fields promoting a weak vortex-stripe coupling, appears at $T > 6K$ and slightly increases with temperature. Reducing H_z changes the direction of the supercurrents and inverts the bright and dark contrast in the diamond-like patterns at the stripe ends near the top edge of the sample. This corresponds to the accumulation of the exiting positive vortices at the inner side of the positive stripe ends and depletion of the vortex density on the side facing the top Nb edge (Fig.8e). When the field is ramped down to $H_z \sim 0$ negative vortices (dark contrast) start entering the sample and

easily pass across the positively charged stripe ends near the top sample edge (Fig.8f). Counterintuitively, there is no effect on the entry of negative vortices from the negatively charged Py stripe ends touching the bottom edge of the Nb film. We suggest that here, the edge barrier regulating the vortex entry in SC films and platelets [22] becomes the dominant factor. The negative magnetic charges at the stripe ends residing at the Nb square edge could enhance the entry barrier for negative vortices. However, we see that this effect is negligible. After their initial entry, the negative H_z -vortices can only be pushed inside the sample by the negative magnetic charges at the stripe ends touching the Nb edge. However, this interaction force decays rapidly with distance. The above results demonstrate that the ends of magnetic stripes overlapping with the edges of the Nb film do not affect vortex entry, independently of their polarity. Therefore, vortex gating effect can be realized only when the magnetic stripe ends are placed at some distance away from the superconducting film edges.

2c. Stripes polarized at 45°

The in-plane field applied along the sample diagonals polarizes the Py stripes at 45° to their length and magnetic charges appear symmetrically at all stripe edges, although the magnetic charge density is $\sqrt{2}$ times smaller than for the purely transverse or longitudinal polarizations. Therefore, one should expect both, albeit weaker effects of guiding and gating for vortices induced by the normal field, H_z . In Fig.9a-d we compare H_z -vortex patterns for four different diagonal orientations of $H_{||}$ emerging at the top side of the stripes, 200 μ m away from the Nb film edge.

At the bottom side, where the Py stripe ends coincide with the edge of the Nb film, the major feature is the vortex guiding effect (similar to Fig.4, not shown). Here, the flux patterns are practically identical for all 4 diagonal polarizations of the stripes. Although, similar to the top side of the Py stripes, they show some left-right asymmetry defined by the sign of the horizontal magnetization component perpendicular to the long stripe edges. The vortex entry from the bottom sample side is practically independent of the vertical (parallel to long stripe edges) magnetization component in the Py stripes. Changing the sign of the magnetic charge at the bottom stripe ends in contact with the Nb film edge does not affect the flux penetration.

At the top edge of the diagonally polarized stripes, the dominating effect is also vortex guiding (see Fig.9a-d where images are presented at $H_z=8$ and 11.5 Oe for each orientation of the in-plane field). However unlike at the bottom ends of the stripes, the top positively charged ends introduce a noticeable barrier for H_z -vortices while negatively charged ends allow unrestricted vortex entry. The overall behavior is a combination of the vortex guiding and pinning effects observed for purely transverse and parallel polarizations of the Py stripes (compare with Figs.9e-h, which show flux patterns for two transverse and two longitudinal orientations of $H_{||}$). The decreased magnetic charge at the edges of the diagonally polarized stripes results in a shallow penetration of H_z -vortices along the stripes and a weaker concentration of B_z on the positive stripe ends. We also observed the left-right asymmetry of vortex density spreading from the gaps into the stripe regions. The asymmetry depends on the polarity of the horizontal component of $H_{||}$, imposing maximum B_z at the positively charged edges, followed by decay of vortex density across the gaps and subsequently into neighboring stripes through their negatively charged edges. This

confirms that positive H_z -vortices are regularly impeded by the positive stripe edges but can easily traverse across the negatively charged edges. The current anisotropy, $J_c^{\parallel}/J_c^{\perp}$, for the diagonally polarized Py strips, following from the position of the SCT lines, is smaller than that of the transversely polarized strips. It increases with temperature qualitatively similar to the current ratios shown in Fig.7.

The above observations show that by rotating the stripe polarization, it is possible to tune vortex guiding and retardation effects. This allows the vortex triode action [8] using our magnetic stripes architecture. However, device implementation will require placing the magnetic stripes inside a superconducting film at some distance from its edges.

Conclusions

We confirm our previous finding [8,9] that soft magnetic stripes, which can be easily polarized along different in-plane directions using small magnetic fields, is a useful tool for manipulating Abrikosov vortices in superconducting/ferromagnetic hybrids. In this work we studied a sample where three sides of the permalloy magnetic stripe array is at a fixed distance away from the superconducting niobium film edge while the fourth side reaches the Nb film edge. With such a geometry, we not only compared the effect of the Py stripes at different distances from the SC edges, but also *quantitatively* estimated the effect of magnetic pinning introduced by the stripes on the average critical currents flowing along and across their length. The main magnetic coupling between the normal Abrikosov vortices and permalloy stripes is defined by magnetic charges at the stripe edges that are proportional to the magnetization component perpendicular to these edges. In a simple scenario, the coupling can be treated as an attraction or repulsion between charged filaments and point-like charges of individual vortices. The resulting effect is vortex guided motion for vortices moving along the charged stripe edges and strong magnetic pinning of vortices moving across the Py stripe edges. The magnetic charge density at the Py stripe edges can be smoothly varied by gradually rotating an in-plane magnetization field, allowing controlled switching between vortex guided motion and gating effects. Magnetically charged Py stripe edges of the same polarity as that of entering H_z vortices provide the largest interaction, while edges of opposite polarity hardly affect the vortex entry and exit. We associate this with dynamics of vortices crossing the oppositely charged edges and confirm our suggestion by modeling the overdamped vortex motion across strongly localized attractive and repulsive potential barriers.

The magnetically charged short ends of Py strips enable flux gating by controlling the penetration of vortices into the gap region between the stripes, depending on the magnetization direction in the stripes. The gating action of the magnetic stripe ends is observed only when the ends of the stripes terminate at some distance away from the superconducting film edge. In contrast, when the stripe ends overlap with the edge of the superconducting film, we find only guided motion of the Abrikosov vortices, while a strong edge barrier becomes more efficient than magnetically charged stripe ends and compromises the gating effect of the stripes. We believe that miniaturization of our architecture, choice of the geometrical parameters (width, gap, distance from the edges of SC elements, and thickness of magnetic stripes), and selection of low-pinning superconducting film will allow creation of structures to manipulate individual vortices.

Acknowledgements

This work was supported by the U.S. Department of Energy, Office of Science, Materials Sciences and Engineering Division. The work of F. Colauto at Argonne National Laboratory was supported by the Sao Paulo Research Foundation FAPESP (grant No. 2015/06.085-3). We used thin film deposition and patterning facilities at the Center for Nanoscale Materials, supported by the U. S. DOE, Office of Science, Office of Basic Energy Sciences, under Contract No. DE-AC02-06CH11357. A.I.B. acknowledges support from French ANR projects "SUPERTRONICS".

Appendix

We model single vortex motion, described by trajectory $x(t)$, across a sharp one-dimensional attractive and repulsive potential using the approximation $U(x)=(-/+)k/(1+x^2)$, which has smooth divergence at $x \rightarrow 0$. The resulting equation of motion under a permanent drive force C will be:

$$-\eta \dot{x} \pm 2kx/(1+x^2)^2 + C = 0$$

Here η is the vortex viscosity, k – the strength of the potential $U(x)$, and $-/+$ correspond to the attractive and repulsive potential U respectively. The reduced form:

$$-\alpha \dot{x} \pm x/(1+x^2)^2 + c = 0$$

with $\alpha = \eta/2k$, $c = C/2k$, has the solution: $(1/c)[x - f(x)] = (1/\alpha)t + \text{const}$, where

$f(x) = -\int x dx / [x + c(1+x^2)^2]$ for repulsive and $f(x) = +\int x dx / [-x + c(1+x^2)^2]$ for attractive $U(x)$.

The numerical solution of the integrals for a chosen c provides an easy way of analyzing the vortex trajectory $x(t)$. In Fig. 10a we show $x(t)$, neglecting the constant and presenting t in units of c/α . At small driving force c , the vortex is delayed near the center of the potential ($x(t)$ turns horizontal, i.e. $\dot{x} \rightarrow 0$). The following segment with negative derivative is unphysical. However, the next stable branch of the solution corresponding to vortex motion on the other side of $U(x)$ can be reached by a jump which is much smaller for the attractive potential. At a critical value of the driving force $c_{cr} = 0.32476$, which is the same for both signs of U , the vortex motion becomes continuous, although the vortex speed is modified differently for $+$ and $-U$ (Fig.10b).

One expects that crossing the attractive barrier is easier than crossing the repulsive barrier. Hence, near the repulsive barrier, the vortices should accumulate and enhance the repulsion of incoming vortices, while they should accelerate and easily traverse the attractive barrier. The dissipation and resulting increase of the local temperature due to vortex acceleration can potentially assist the facile crossing of the attractive barrier.

References

- [1] H. Toepfer, and T. Ortlev, Design infrastructure for rapid single flux quantum circuits, *Cryogenics* **49**, 643 (2009).
- [2] S. Anders, M.G. Blamire, F.-Im. Buchholz, D.-G. Cr  t  , R. Cristiano, P. Febvre, L. Fritzsche, A. Herr, E. Il'ichev, J. Kohlmann, J. Kunert, H.-G. Meyer, J. Niemeyer, T. Ortlev, H. Rogalla, T. Schurig, M. Siegel, R. Stolz, E. Tarte, H. J.M.ter Brake, H. Toepfer, J.-C. Villegier, A. M. Zagorkin, A. B. Zorin., European roadmap on superconductive electronics – status and perspectives, *Physica C* **470**, 2079 (2010).

- [3] O. A. Mukhanov, Energy-Efficient Single Flux Quantum Technology, *IEEE Trans. Appl. Supercond.* **21**, 760 (2011).
- [4] K. K. Likharev, Superconductor digital electronics, *Physica C* **482**, 6 (2012).
- [5] J. Kunert, O. Brandel, S. Linzen, O. Wetzstein, H. Toepfer, T. Ortlepp, and H.-G. Meyer, Recent Developments in Superconductor Digital Electronics Technology at FLUXONICS Foundry, *IEEE Trans. Appl. Supercond.* **23**, 1101707 (2013).
- [6] D. S. Holmes, A. L. Ripple, and M. A. Manheimer, Energy-Efficient Superconducting Computing—Power Budgets and Requirements, *IEEE Trans. Appl. Supercond.* **23**, 1701610 (2013).
- [7] T. Golod, A. Iovan, and V. M. Krasnov, Single Abrikosov vortices as quantized information bits, *Nat. Comm.* **6**, 8628 (2015).
- [8] V. K. Vlasko-Vlasov, F. Colauto, T. Benseman, D. Rosenmann, and W.-K. Kwok, Triode for magnetic flux quanta, *Sci. Rep.* **6**, 36847 (2016).
- [9] V. K. Vlasko-Vlasov, F. Colauto, A. I. Buzdin, D. Rosenmann, T. Benseman, and W.-K. Kwok, Magnetic gates and guides for superconducting vortices, *Phys. Rev. B* **95**, 144504 (2017).
- [10] I. F. Lyuksyutov and V. L. Pokrovsky, Ferromagnet/superconductor hybrids, *Adv. Phys.* **54**, 67 (2005).
- [11] M. Velez, J. I. Martin, J. E. Villegas, A. Hoffman, E. M. González, J. L. Vicent, and I. K. Schuller, Superconducting vortex pinning with artificial magnetic nanostructures, *J. Magn. Magn. Mater.* **320**, 2547 (2008).
- [12] A. Yu. Aladyshkin, A. V. Silhanek, W. Gillijns, and V. V. Moshchalkov, Nucleation of superconductivity and vortex matter in superconductor/ferromagnet hybrids, *Supercond. Sci. Technol.* **22**, 053001 (2009).
- [13] V. V. Moshchalkov and J. Fritzsche, *Nanostructured Superconductors*, World Scientific, Singapore (2011).
- [14] J. Brisbois, M. Motta, J. I. Avila, G. Shaw, T. Devillers, N. M. Dempsey, S. K. P. Veerapandian, P. Colson, B. Vanderheyden, P. Vanderbemden, W. A. Ortiz, N. D. Nguyen, R. B. G. Kramer, and A. V. Silhanek, Imprinting superconducting vortex footsteps in a magnetic layer, *Sci. Rep.* **6**, 27159 (2016).
- [15] C. Reichhardt and C. J. Olson Reichhardt, Transverse ac-driven and geometric ratchet effects for vortices in conformal crystal pinning arrays, *Phys. Rev. B* **93**, 064508 (2016).

- [16] M. Trezza, C. Cirillo, A. L. Dolgii, S. V. Redko, V. P. Bondarenko, A. V. Andreyenka, A. L. Danilyuk, S. L. Prischepa, and C. Attanasio, Change of the topology of a superconducting thin film electromagnetically coupled with an array of ferromagnetic nanowires, *Supercond. Sci. Technol.* **29**, 015011 (2016).
- [17] O.V. Dobrovolskiy, Abrikosov fluxonics in washboard nanolandscapes, *Physica C* **533**, 80 (2016).
- [18] Z. Adamus, M. Cieplak, M. Konczykowski, L. Y. Zhu, and C. L. Chien, Influence of magnetic domain landscape on the flux dynamics in superconductor/ ferromagnet bilayers, *Phys. Rev. B* **93**, 054509 (2016).
- [19] V. K. Vlasko-Vlasov, G. W. Crabtree, U. Welp, and V. I. Nikitenko, Magneto-optical studies of magnetization processes in high-Tc superconductors, *NATO ASI Ser., Ser. E* **356**, 205 (1999).
- [20] G. Carneiro and E. H. Brandt, Vortex lines in films: Fields and interactions, *Phys. Rev. B* **61**, 6370 (2000).
- [21] J. I. Vestgarden, D.V. Shantsev, A.A. F. Olsen, Y. M. Galperin, V.V. Yurchenko, P. E. Goa, and T. H. Johansen, Interaction between Superconducting Vortices and a BlochWall in Ferrite Garnet Films, *Phys. Rev. Lett.* **98**, 117002 (2007).
- [22] E. H. Brandt, G. P. Mikitik, and E. Zeldov, Two Regimes of Vortex Penetration into Platelet-Shaped Type-II Superconductors, *J. Exper. Theor. Phys.* **117**, 439 (2013).

Figures

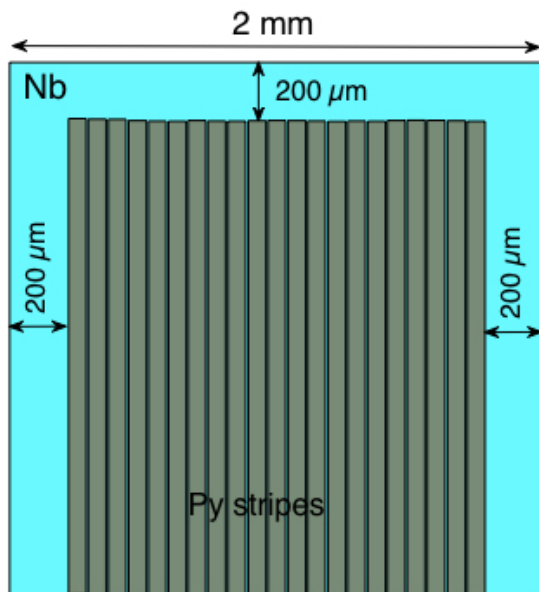


Fig.1 Schematic of the sample. 2x2mm 100nm thick Nb film is covered with 15nm thick SiO₂ and an array of 30μm wide, 40nm thick Py stripes with 2 μm gaps is deposited on top as shown. The bottom end of the Py pattern coincides with the Nb film edge. 200 μm bands of Nb film remain bare at three other sides.

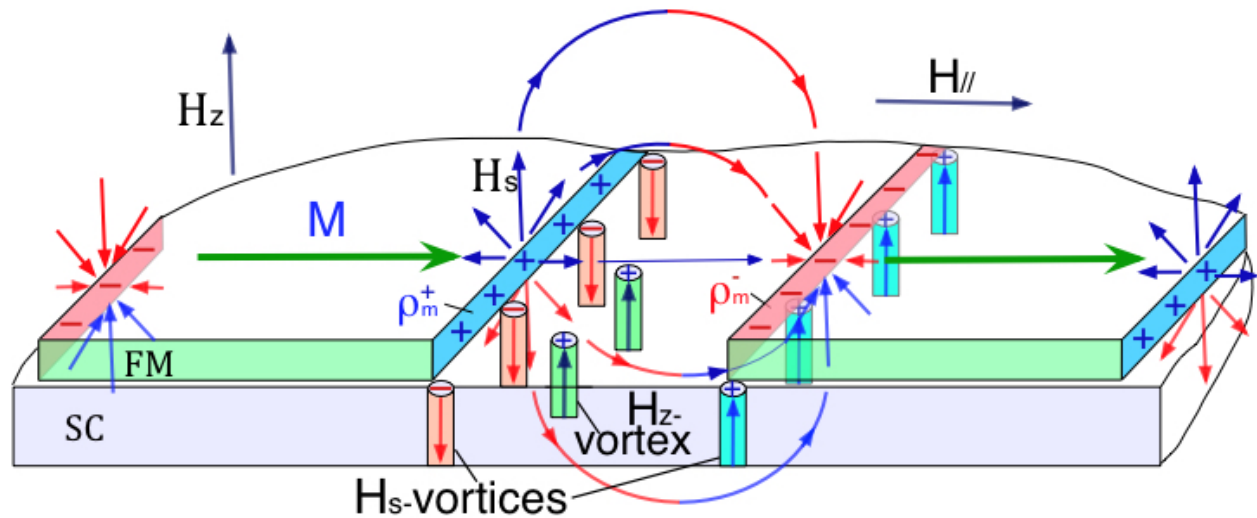


Fig.2 Schematic of magnetic charges (ρ_m) and stray fields (\mathbf{H}_s) at the edges of the transversely polarized FM stripes. The vortex distribution corresponds to the initial application of a small normal field H_z . \mathbf{M} is the magnetization vector of the stripe. Edges of the thin stripes perpendicular to \mathbf{M} act as magnetically charged filaments, such that the \mathbf{H}_s -vectors are directed perpendicular to these filaments in the vicinity of the edges. Cooling below T_c produces stray field generated H_s -vortices. In addition, the normal field (H_z) applied below T_c will generate H_z -vortices. $H_{||} \ll M$.

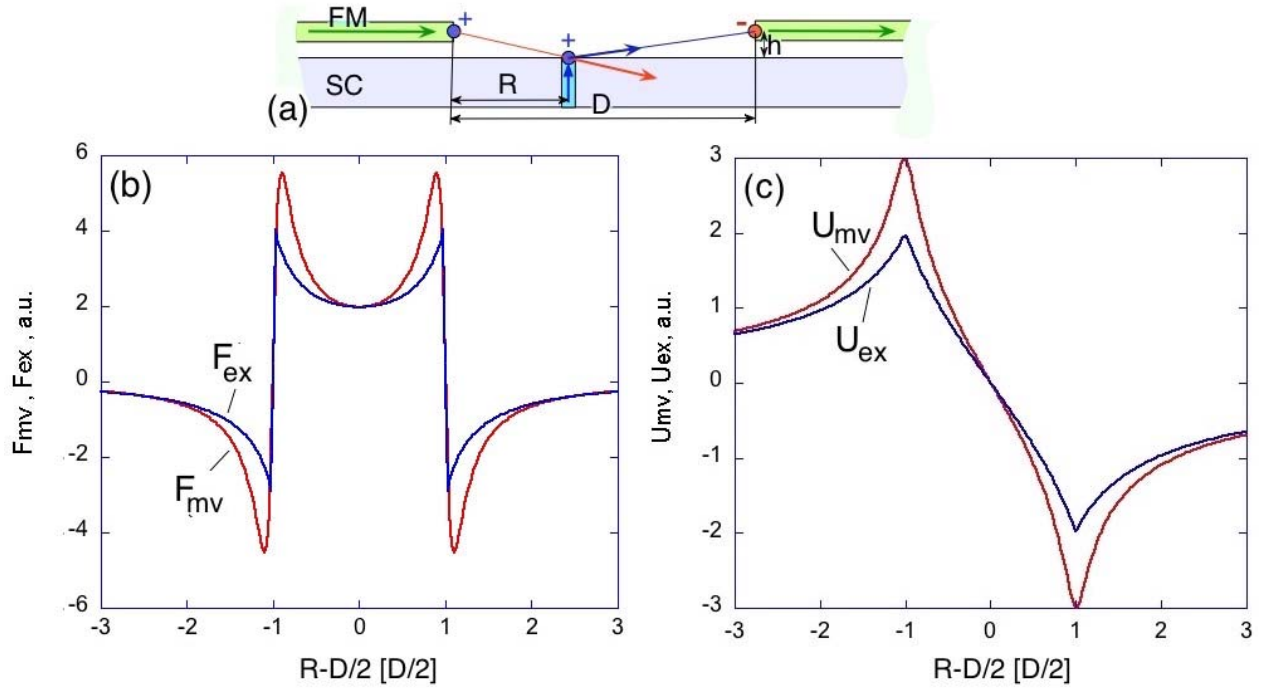


Fig.3 (a)-Schematic of magnetic charges at the edges of the transversely polarized FM strips and appropriate forces on the positive Abrikosov vortex. (b)- Calculated vortex/edge interaction forces F_{mv} (eq.1) and F_{ex} –exact solution accounting for Meissner screening (eq.2). The numerical data for F_{ex} are multiplied by 2.5 to match curves at $R-D/2=0$. (c) Interaction potentials U_{mv} (for F_{mv}) and U_{ex} (for F_{ex}).

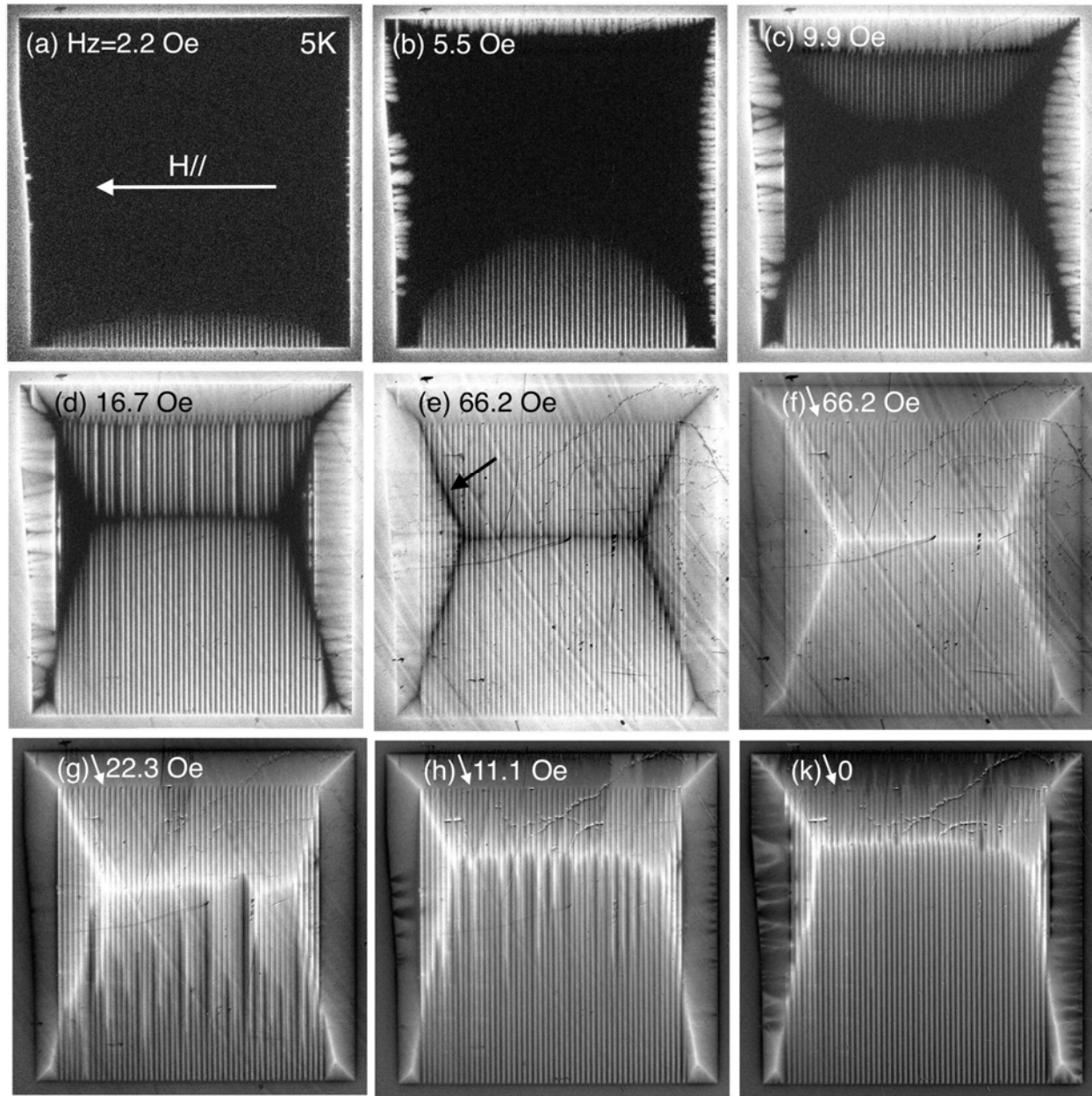


Fig.4 Successive images of the normal flux entry and exit upon increasing (a-e) and decreasing (f-k) perpendicular field H_z at $T=5K$ in the sample with transversely polarized stripes. Black arrow in (e) points to the sharp current turn (SCT) line referred to in the text.

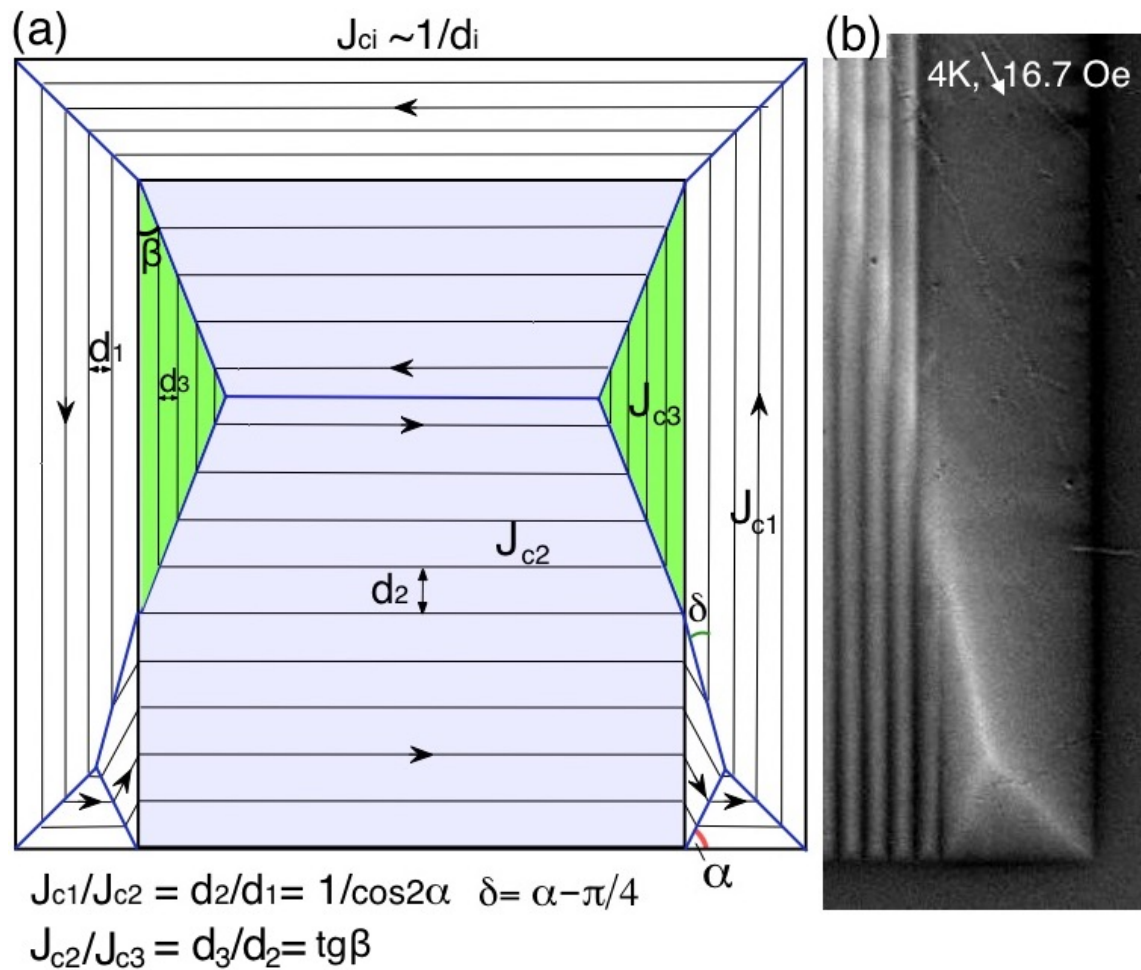


Fig.5 Arrangement of the sharp current turn (SCT) lines in the total critical state: (a)-current flow scheme in the sample and (b)-the MO image near the right sample side. Angles of the SCT lines are defined by the ratios of the critical currents in the bare SC film (J_{c1}), currents flowing in the Py stripe patterned area across the stripes (J_{c2}), and currents along the stripes (J_{c3}). Distances between the current lines in different regions are inversely proportional to the current densities. From the geometry of the continuous current flow, one finds relations between J_{ci} and angles of the SCT lines as shown in the picture. Angles α and δ are not independent, which allows estimates of the current ratios using both angles obtained from the experimental MO pictures.

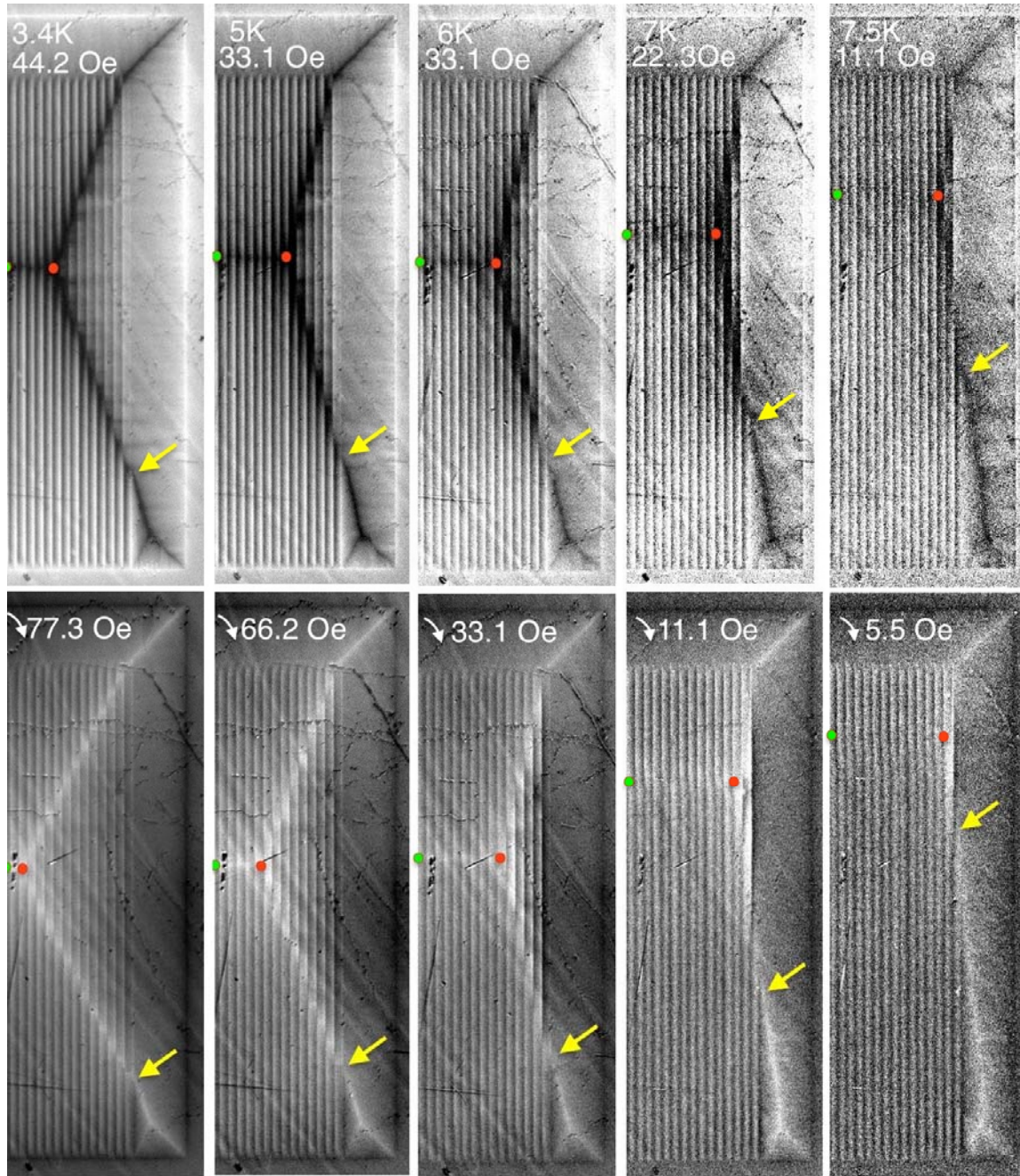


Fig.6 Position of the SCT lines near the right sample side at different temperatures with increasing (top row) and decreasing (bottom row) normal fields, H_z . The total critical state (critical flux gradients form over the entire sample area) is achieved at different applied fields H_z decreasing with T . Images at fields slightly larger than the total penetration field (top row) are chosen for illustration of the SCT lines. Position of the horizontal SCT line is marked by the small green circle and crossing of the tilted SCT lines in the patterned area- is marked by red circle. Yellow arrows point to the crossing of the tilted SCT line in the bare Nb film with the edge of the patterned region.

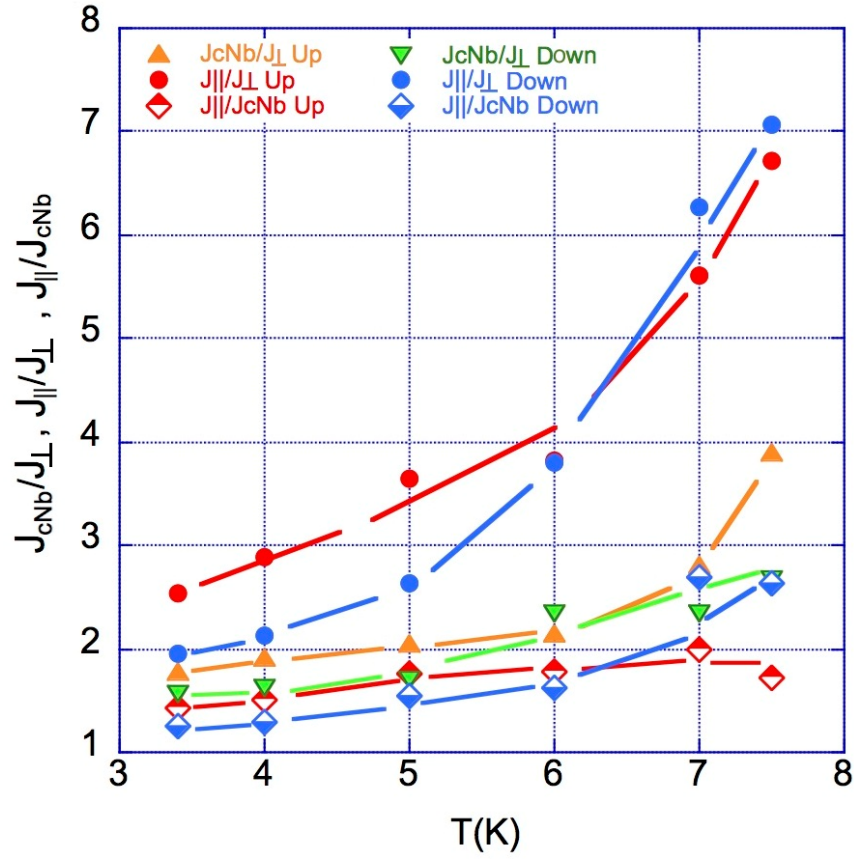


Fig.7 Ratios of the critical currents in the bare Nb film (J_{cNb}), and in the patterned area flowing across (J_{\perp}) and along the Py stripes (J_{\parallel}) at different temperatures. Symbols Up and Down correspond to ratios from MO patterns obtained with increasing and decreasing H_z .

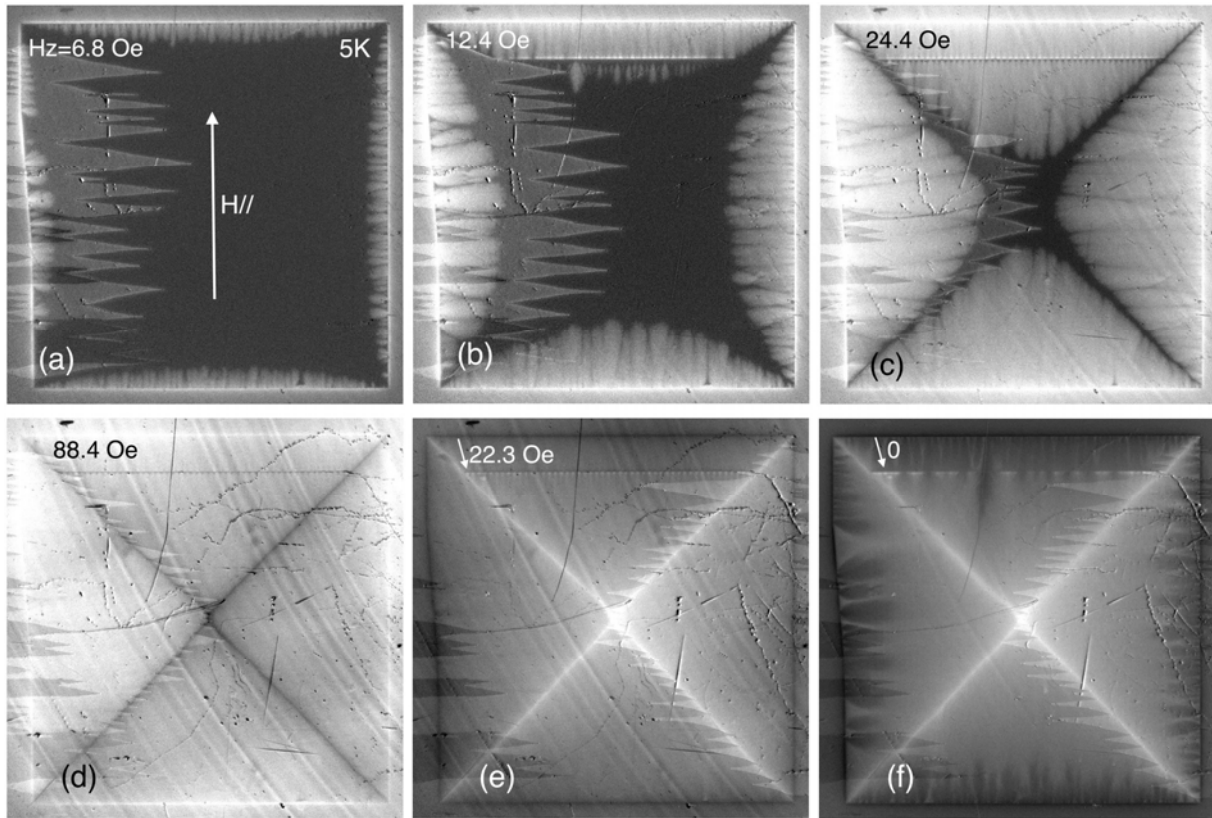


Fig.8 Vortex entry and exit in the sample with longitudinally polarized stripes at $T=5\text{K}$. H_z increases in (a-d) and decreases in (e-f)

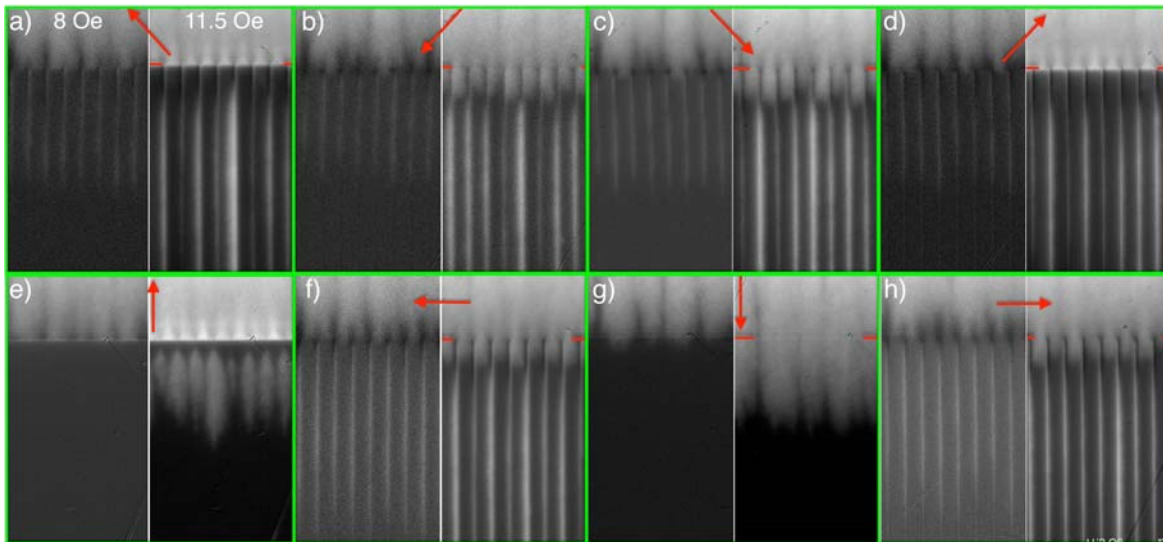


Fig.9 Normal flux entry at different polarizations of the Py stripes. Top row (a-d) shows images for four diagonal in-plane fields, and bottom row (e-h) illustrates 2 horizontal and 2 vertical polarizations indicated by red arrows. For each polarization, there are two successive images taken at $H_z=8$ (left) and 11.5 Oe (right) respectively. $T=5\text{K}$.

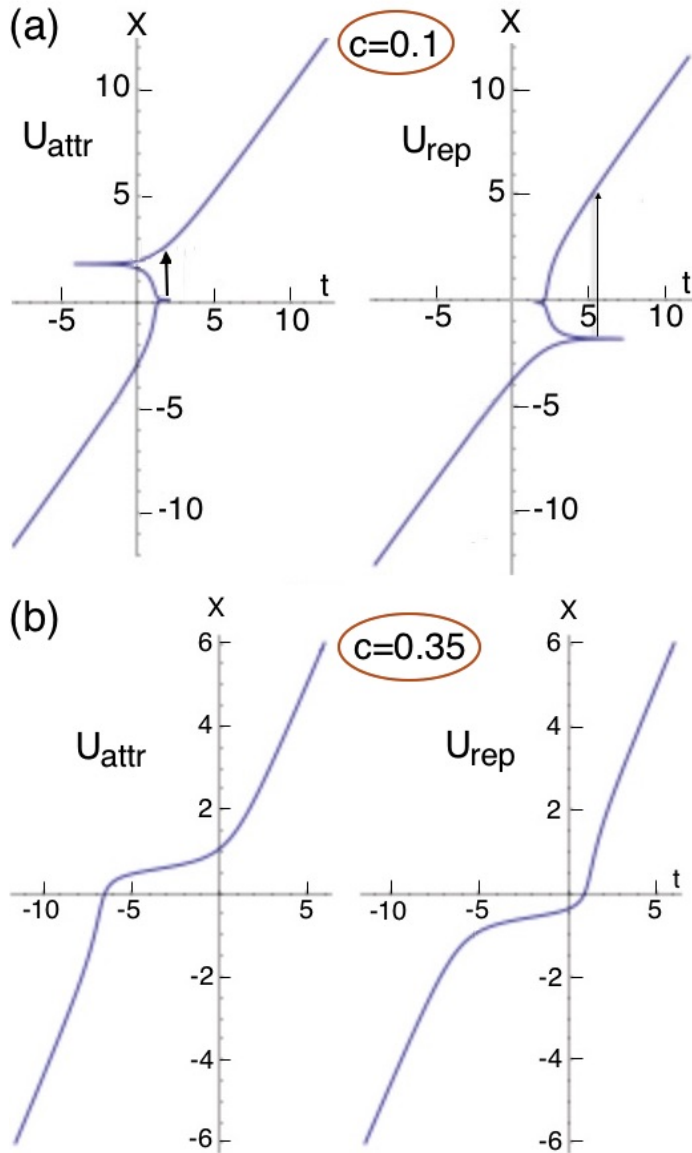


FIG.10 Trajectories $X(t)$ of the vortex motion across the attractive (left) and repulsive (right) 1D potentials, $U(x)=\pm k/(1+x^2)$, under the action of a constant drive (a) $c=0.1$, and (b) above the critical drive $c>c_{cr}=0.32476$ when vortex motion becomes continuous. At $c<c_{cr}$ the vortex is delayed near the center of the potential and then can jump to the second continuous motion branch. The delay (horizontal segment of $X(t)$) and the jump (shown by arrow) are essentially longer for the repulsive potential. The intermediate segment with $dX/dt<0$ is not physical. X is in arbitrary units and t is in units of c/α .